2024 European Control Conference (ECC)
June 25-28, 2024. Stockholm, Sweden

Optimal operation of pumped thermal energy storage for simultaneous peak shaving and voltage control in multi-energy system

Zhengfa Zhang, Yiqiao Xu, Corneliu Arsene, Yixing Liu, Alessandra Parisio

Abstract— **The integration of a large share of renewable generation poses growing challenges to the safe and reliable operation of modern energy systems. Utilizing large scale energy storage is an effective way to accommodate high penetration of renewable energy. Compared with other large-scale energy storage technologies, such as pumped storage hydropower and compressed air energy storage, pumped thermal energy storage (PTES) has significantly higher energy density and less space requirements. Furthermore, PTES is able to integrate multiple energy networks, e.g., electric and heating, which is an additional source of flexibility. In this paper, the use of a PTES to provide simultaneous peak shaving and voltage control in multi-energy systems (MES) is explored and an operation optimization framework is developed. In the proposed framework, the operating characteristics of the PTES are linearized, and the dynamics of the PTES are handled by a model predictive control (MPC) scheme. The overall optimization problem is formulated as a mixed-integer nonlinear problem. The performance of the proposed optimization framework is verified through realistic case studies and the potential benefits of the PTES to support more sustainable grid operation is demonstrated.**

I. Introduction

In recent years, to achieve the ambition of net-zero carbon emissions, the share of renewable energy sources (RES) is growing rapidly in today's energy pattern [1]. Compared with traditional fossil fuels, the RES are high intermittent and unstable, posing great challenges to the safe and reliable operation of power grid [2].

Multi-energy system (MES) is one of the effective solutions to overcome the above challenges [3]. By coordinating and co-optimizing the electric power grid with other energy networks, e.g., heating and cooling, MES can leverage the flexibility between different energy vectors. Within this context, the fifth-generation district heating and cooling (5G-DHC) networks have received growing attention due to the advantages of more efficiently meeting both heating and cooling demands. Heat losses is significantly reduced in 5G-DHC network, as it can operate at temperature close to surroundings [4].

The deployment of large scale energy storage systems to provide grid services is another effective solution to accommodate high penetration of RES [5]. Typical technologies include pumped storage hydropower (PSH) and compressed air energy storage (CAES). However, these technologies have high requirement on geographical space, and the energy density is relatively low [6].

An emerging technology to overcome the above limitations is pumped thermal energy storage (PTES) [7]. PTES uses low-cost excess electricity to operate as a heat pump that charges a hot storage and/or extract heat from a cold storage. Then, the stored thermal energy is discharged to drive a thermodynamic heat engine to generate electricity when there is high demand [8]. In addition, PTES can be used as multi-energy thermally-integrated PTES (mTIPTES) to improve the whole system efficiency. Even though several studies on the operation of PTES or mTIPTES are available, they focus on thermodynamic analysis and modeling, and on the device level. Therefore, the optimal use of a PTES, and the resulting potential benefits, to provide grid services has not been explored yet. Furthermore, the interaction of a PTES with a MES is seldom reflected in current research [9] [10] [11] [12].

Peak shaving and voltage support are two fundamental electric grid services to ensure reliable operation of power grid. Peak shaving is needed in order to flatten the load profile as much as possible, by reducing the peak electric load and shift it to times of lower electric power demand, typically by using energy storage systems or demand side management strategies [13]. Peak shaving can help improve power quality, ensure efficient energy utilization and reduce energy cost. As to voltage regulation, the main objective is to maintain the network feeder voltages within the allowed range by scheduling voltage regulation devices, e.g. on-load tap changers (OLTCs), capacitor banks (CBs) or the reactive power output of DG inverters [14].

Conventionally, peak shaving and voltage regulation are usually performed separately (see [13] and [14]). However, recent studies reveal that these two grid services have mutual impacts on each other. For instance, reshaping load curves have influence on voltage profile, especially for low-voltage feeders with high R/X ratio, and regulating voltages also results in reduction of peak load [15] [16]. Very few studies explored the co-operation of peak shaving and voltage control [16] [17], but these works focus only on the electric power grid and utilize traditional battery energy storage systems, instead of the new PTES technology and multiple energy networks within a MES scenario.

In this paper, a contribution to fill this gap is provided, by exploring the utilization of PTES to provide both peak shaving and voltage control within a MES. Compared with previous work, the main contributions of this paper are summarized as follows,

This work was partially supported by the projects Supergen Energy Networks Impact Hub 2023, EPSRC, EP/Y016114/1, start date: October 2023, and GRIPHS: Grid Integration of Pumped Heat Energy Storage Systems, EPSRC, EP/W027860/1, start date: November 2022. The authors are with the Department of Electrical and Electronic Engineering, University of Manchester, Manchester M13 9PL, U.K. (e-mail: alessandra.parisio@manchester.ac.uk).

- A co-optimization framework is proposed to use a PTES as a mTIPTES to provide peak shaving and voltage control in MES. This framework aims at minimizing the overall operation cost while satisfying operation constraints, including the ones of the MES and PTES devices.
- The operating characteristics of mTIPTES are linearized and the overall optimization framework is formulated as a mixed-integer nonlinear programming (MINLP) problem. The dynamics of mTIPTES device are controlled by using an MPC scheme.
- For additional network flexibility, the system level interaction between mTIPTES and MES is captured and optimally managed by the proposed framework.

The remainder of this paper is organized as follows. The modeling of studied system is provided in Section II while the formulation of the optimization framework is given in Section III. Case studies are provided in Section IV and finally Section V concludes the paper.

II. System Modeling

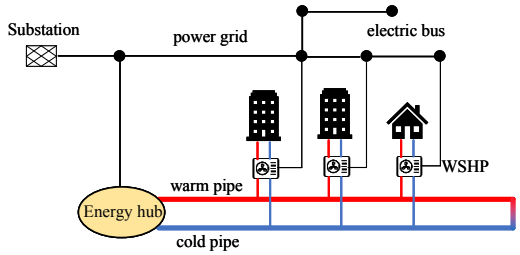

Fig. 1. Multi-energy Framework

The diagram of a typical MES consisting of a distribution network (DN) and 5G-DHC network is shown in Fig. 1. The main components of the 5G-DHC network include cold and warm bidirectional pipes, water source heat pumps (WSHP) and an energy hub. The WSHP consumes electric energy to provide heating or cooling to end users and the energy hub is responsible for maintaining the network energy balance. In the following content of this section, the detailed modeling of DN and 5G-DHC network are introduced in detail.

A. Modeling of DN

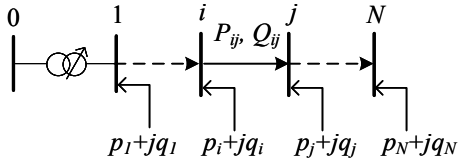

Fig. 2. Topology of DN.

The topology of a typical radial DN is shown in Fig. 2, which is represented by $\mathcal{G} = (\mathcal{N}, \mathcal{L})$, where $\mathcal{N} := \{0, 1, ..., N\}$ denotes the set of buses, while $\mathcal{L} := \{1, ..., N\}$ denotes the set of branches. For each bus $i \in \mathcal{N}$, let $s_i = p_i + \boldsymbol{i}q_i$ denote its complex power injection. For each branch $(i, j) \in \mathcal{L}$, let $z_{ij} = r_{ij} + \boldsymbol{i}x_{ij}$ denote its impedance and $S_{ij} = P_{ij} + \boldsymbol{i}Q_{ij}$ be the complex power flowing from bus i to j. The power flow can be described by the well-known and widely used linear Distflow equations [18]

$$P_{ij} = \sum_{k \in \mathcal{C}_j} P_{jk} - p_j, \tag{1a}$$

$$Q_{ij} = \sum_{k \in \mathcal{C}_j} Q_{jk} - q_j, \tag{1b}$$

$$v_i - v_j = 2\left(r_{ij}P_{ij} + x_{ij}Q_{ij}\right), \tag{1c}$$

where v_i represents the squared voltage magnitude of bus i and $\mathcal{C}_j$ represents the set of the downstream buses of bus j. The linear DistFlow equations assume the voltage drops and line power flows to be approximately linearly related to power injections, and their approximation accuracy depends on the loading conditions; however, any alternative convex relaxation of the power flow equations can be used in the proposed framework.

B. Modeling of 5G-DHC Network

The 5G-HDC modeling approach adopted in this paper is inspired to the one presented in [19], which allows the operation of 5G-DHC network to be convexified by linear programming (LP), hence to be efficiently handled. The 5G-DHC network is modeled by two sets of energy balancing equations, the node energy balance equation and the network energy balance equation. In addition, the interactions among the DN, the mTIPTES and the 5G-DHC network are also captured. In this section, the modeling of the 5G-HDC and its main components is described.

1) WSHP: The WSHP generates heating or cooling by consuming electricity. The performance for heating or cooling performance is given by a coefficient of performance (COP) or an energy efficiency ratio (EER), respectively

$$Q_{h,hp} = COP_{hp} \cdot P_{hp}, \tag{2a}$$

$$Q_{h,hp} \leqslant \overline{Q}_{h,hp}, \tag{2b}$$

$$Q_{c,hp} = EER_{hp} \cdot P_{hp}, \tag{2c}$$

$$Q_{c,hp} \leqslant \overline{Q}_{c,hp}, \tag{2d}$$

where $Q_{h,hp}/Q_{c,hp}$ represents the heating/cooling energy generated by the WSHP, $\overline{Q}_{h,hp}/\overline{Q}_{c,hp}$ is the nominal heating/cooling capacity of the WSHP. P_{hp} is the electric power consumed by the WSHP. In this paper, we can assume constant COP/EER, which is a reasonable assumption for the considered the WSHP operational range [19] [20].

2) Pipes: The operating temperature of the 5G-DHC network is close to the one of the surroundings, therefore pipes in the 5G-DHC network are usually not insulated. The thermal losses of the warm and cold pipes through the surrounding soil can be approximated with the following group of linear equations [19]

$$Q_{h,loss} = (kA)\left(T_h - T_{soil}\right), \tag{3a}$$

$$Q_{c,loss} = (kA)\left(T_{soil} - T_c\right), \tag{3b}$$

where $Q_{h,loss}$ and $Q_{c,loss}$ represent the thermal losses in the warm and cold pipe, respectively. (kA) denotes the thermal transmittance including all heat transfer resistances from the fluid to the soil. T_h, T_c and T_{soil} represent the temperature of the warm pipe, cold pipe and the surrounding soil respectively.

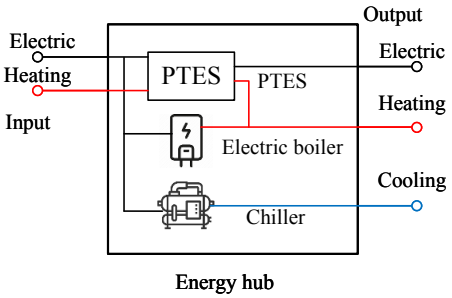

Fig. 3. Energy hub configuration.

3) Energy Hub: The configuration of an energy hub is shown in Fig. 3, where an mTIPTES, an electric boiler and a chiller are included. The energy hub takes electric and heating as inputs while providing electric, heating and cooling as outputs. In this paper, a hot mTIPTES is considered, which can take both electric and heating as both inputs and outputs [12]. In addition, the electric boiler and chiller can provide additional heating or cooling when needed, so that the network heating and cooling energy can be balanced.

The electric boiler consumes electricity to generate heating energy; the relationship between the thermal output $Q_{h,eb}$ and the electric input P_{eb} is given as

$$Q_{h,eb} = P_{eb}\eta_{eb}, \tag{4a}$$
$$Q_{h,eb} \leqslant \overline{Q}_{h,eb}, \tag{4b}$$

where $\overline{Q}_{eb}$ is the nominal capacity of the electric boiler and η_{eb} is the thermal efficiency, which is assumed to be constant.

On the other hand, cold is provided by an electric chiller, whose equations are expressed as

$$Q_{c,cc} = COP_{cc} \cdot P_{cc}, \tag{5a}$$
$$Q_{c,cc} \leqslant \overline{Q}_{cc}, \tag{5b}$$

where $Q_{c,cc}$ and P_{cc} are the cooling output and the electric input of the electric chiller, respectively. $\overline{Q}_{cc}$ is the electric chiller's nominal capacity.

In the hot mTIPTES, the key components are the high-temperature heat pump (HTHP), the organic Rankine cycle (ORC) and the hot thermal energy storage (HTES) using Phase Change Materials (PCMs). The HTHP converts electrical energy into thermal energy, which is stored in the HTES, while the ORC transforms the stored thermal energy into electric power when needed. The HTHP and the ORC can be modeled by using the following equations [21]

$$Q_{h,z} = g_z(\cdot) P_z, \tag{6a}$$
$$k_z \underline{\alpha}_z \overline{P}_z \leqslant P_z \leqslant k_z \overline{P}_z, \tag{6b}$$
$$Q_{h,z} \leqslant k_z \overline{Q}_{h,z}, \tag{6c}$$

where z represents either the HTHP or the ORC, $Q_{h,z}$ and P_z are the thermal energy and electric energy of the components, while $\overline{Q}_{h,z}$ and $\overline{P}_z$ are their nominal values. $g_z(\cdot)$ represents the non-linear operating characteristics of the corresponding components, which is the COP for the HTHP and the reciprocal of the efficiency η_{ORC} for the ORC. k_z is a binary variable that represents the on/off status of the components. The linear approximations of the non-linear characteristics for the HTHP and the ORC are given as

$$\frac{Q_{h,z}}{\overline{Q}_{h,z}} \leqslant a_{z,j}\frac{P_z}{\overline{P}_z} + b_{z,j} - b_{z,j}(1-k_z), \tag{7a}$$
$$\frac{Q_{h,z}}{\overline{Q}_{h,z}} \geqslant a_{z,j}\frac{P_z}{\overline{P}_z} + b_{z,j} - b_{z,j}(1-k_z), \tag{7b}$$

where (7a) is the linear approximation for the HTHP and (7b) for the ORC.

The modelling equations for the HTES are given as

$$Q^{ch}_{HTES} \leqslant \gamma_{ch}\overline{Q}^{ch}_{HTES}, \tag{8a}$$
$$Q^{dis}_{HTES} \leqslant \gamma_{dis}\overline{Q}^{dis}_{HTES}, \tag{8b}$$
$$\gamma_{ch} + \gamma_{dis} \leqslant k_{HTES}, \tag{8c}$$
$$SOC(t) = SOC(t-1) + \frac{\Delta t}{C_z}\left[Q^{ch}_{HTES}(t) - Q^{dis}_{HTES}(t)\right], \tag{8d}$$
$$SOC_{\min} \leqslant SOC \leqslant SOC_{\max}, \tag{8e}$$

where Q^{ch}_{HTES} and Q^{dis}_{HTES} represent the charging/discharging heat flows of the HTES, $\overline{Q}^{ch}_{HTES}$ and $\overline{Q}^{dis}_{HTES}$ are their nominal value. γ_{ch} and γ_{dis} are binary variables indicating the charging/discharging status of the HTES; (8c) imposes that charging and discharging do not occur simultaneously. $SOC_{\min}$ and $SOC_{\max}$ denote the min/max state of charge (SOC) levels of the HTES.

The charging/discharging heat flow rate for the PCM thermal storage is a non-linear function of the amount of melted/solidified material. This non-linear function of the HTES can be linearized as [21]

$$Q^{ch}_{HTES} \leqslant a^{ch}_{HTES} \cdot SOC + b^{ch}_{HTES}, \tag{9a}$$
$$Q^{dis}_{HTES} \leqslant a^{dis}_{HTES} \cdot SOC + b^{dis}_{HTES}. \tag{9b}$$

The linear approximation above allow for a computationally efficient way to model the non-linear operating characteristics of the HTHP, ORC and HTES, since only a limited number of linear constraints are added to the problem formulation [21] [22]. In this paper, the data for these linear approximations is obtained from [21].

The thermal energy stored in the HTES can also be used to provide direct heating to the 5G-DHC network. When the HTES directly heats the 5G-DHC network, the following equation is to be considered

$$Q_{h,PTES} \leqslant \overline{Q}_{h,PTES}, \tag{10}$$

where $Q_{h,PTES}$ is the heating energy flow from the mTIPTES to the 5G-DHC network, and $\overline{Q}_{h,PTES}$ is the maximum heat energy flow rate.

4) Energy balance equations: In this section, the energy balance equations for each thermal node and the whole MES network are introduced. For each thermal node i, the balancing equations for heating and cooling are expressed as

$$Q_{h,hp,i} + Q_{h,eb,i} + Q_{h,PTES,i} = Q_{hl,i} + Q^{ch}_{HTES,i}, \tag{11a}$$
$$Q_{c,cc,i} + Q_{c,hp,i} = Q_{cl,i}, \tag{11b}$$

where $Q_{hl,i}$ and $Q_{cl,i}$ are the heating and cooling demands at node i, respectively.

The residual thermal demand should be met by the overall 5G-DHC network. The residual thermal demand at node i is given as

$$Q_{res,i} = Q_{h,hp,i}(1 - COP_{hp,i}^{-1}) - Q_{c,hp,i}(1 + EER_{hp,i}^{-1}) - Q_{c,cc,i}(1 + COP_{cc,i}^{-1}). \quad (12)$$

The residual thermal demand can take positive or negative values. A positive demand means that heat flows from the network to the building, and a negative residual thermal demand indicates a heat flowing from building to the network.

In order to balance the network temperature, the energy hub should cover the residual thermal demand in the whole network and the thermal losses, i.e.,

$$Q_{eh,i} = \sum_{i \in \mathcal{H}} Q_{res,i} + Q_{h,loss,i} - Q_{c,loss,i}, \quad (13)$$

where $\mathcal{H}$ represents the set of all thermal nodes in the 5G-DHC network.

Further, (13) can be rewritten as

$$Q_{h,eb} + Q_{h,PTES} - Q_{h,HTHP}^{ch} - Q_{c,cc} = \sum_{i \in \mathcal{H}} Q_{res,i} + Q_{h,loss} - Q_{c,loss}. \quad (14)$$

For the coupling of the DN and the 5G-DHC network, the electric demand at node i in the 5G-DHC network should be met by the DN

$$P_i = P_{eb,i} + P_{hp,i} + P_{cc,i} + P_{HTHP,i} - P_{ORC,i}. \quad (15)$$

III. MPC-BASED OPERATION OPTIMIZATION FRAMEWORK

In this section, the formulation of the optimization framework to utilize the mTIPTES for simultaneous peak shaving and voltage regulation is introduced. The overall objective is to minimize the operation cost of the whole MES while respecting operational and technical constraints, including constraints on the DN operation, on the 5G-DHC network operation, as well as on the mTIPTES operation. The optimization problem is formulated as an MINLP, and it is embedded into an MPC scheme, so as to take advantage of available forecasts of load demands and energy prices and the inherent feedback mechanism of the MPC, which allows to re-optimize at each appropriate sampling period, over a shifted prediction horizon and with updated forecasts.

A. Objective Function

The proposed framework aims at minimizing the operation cost of the whole MES, which is also the cost of the electric energy purchase. The objective function is expressed as

$$f = \sum_{t=1}^{T} c_{el} P_{el}(t) \cdot \Delta t, \quad (16)$$

where c_{el} is the electric energy price and P_{el} is the feed-in power from the substation, Δt is the sampling period.

B. DN Operation Constraints

The DN operation constraints include the DN power flow and the DG inverter operation constraints. In this paper, the DG inverters are assumed to operate at maximum power point tracking mode (MPPT). Thus, the voltage regulation is achieved by the dispatch of reactive power output of the DG inverters as well as the charging/discharging of the mTIPTES system. The overall operation constraint for DN operation at time instant t is expressed as

$$P_{ij}(t) = \sum_{k \in \mathcal{C}_j} P_{jk}(t) - p_j(t), \quad (17a)$$

$$p_i = p_{g,i}(t) - p_{l,i}(t) - P_i(t), \quad (17b)$$

$$Q_{ij}(t) = \sum_{k \in \mathcal{C}_j} Q_{jk}(t) - q_j(t), \quad (17c)$$

$$q_i(t) = q_{g,i}(t) - q_{l,i}(t), \quad (17d)$$

$$v_i(t) - v_j(t) = 2(r_{ij} P_{ij}(t) + x_{ij} Q_{ij}(t)), \quad (17e)$$

$$\underline{v} \leqslant v_i(t) \leqslant \overline{v}, \quad (17f)$$

$$\overline{q}_{g,i}(t) = -\underline{q}_{g,i}(t) = \sqrt{S_g^2(t) - p_{g,i}^2(t)}, \quad (17g)$$

$$\underline{q}_{g,i}(t) \leqslant q_{g,i}(t) \leqslant \overline{q}_{g,i}(t), \quad (17h)$$

$$P_{el}(t) = P_{01}(t), \quad (17i)$$

where $p_{g,i}$ and $q_{g,i}$ are the real and reactive power outputs from DG inverters, $p_{l,i}$ and $q_{l,i}$ are the real and reactive electric load demands in the DN, respectively. $\underline{v}$ and $\overline{v}$ denote the upper/lower voltage limits, S_g is the nominal capacity of DG inverters.

In addition, to achieve peak shaving, a hard constraint is added to the DN peak load

$$p_{el}(t) \leqslant P_{peak}, \quad (18a)$$

where P_{peak} is the allowed peak. The peak shaving is achieved by the joint operation of the HTHP and the ORC. The excess electric power can be stored in the HTES as thermal energy and the stored thermal energy can be transformed back into electric power to support the peak load. In this way, the network peak load is reduced.

C. Remark on Uncertainty Handling

The operation of a mTIPTES inevitably involves uncertainty, e.g., net-load forecast errors because of uncertainty in RES generation and energy demands. A stochastic MPC (SMPC) approach, which incorporates a probabilistic description of uncertainties and resulting probabilistic constraints, i.e., chance constraints, can be adopted so as to obtain a more robust control of the mTIPTES operation. A major issue of SMPC is the non-convexity brought by the probabilistic constraints, making the quest for an exact solution computationally intractable. In this regard, a possible approach to be adopted is scenario-based MPC (SBMPC), which is a data-driven approach to optimization under uncertainty, able to approximate the SMPC problem using a finite number of scenarios. It is fundamental to compute a number of scenarios sufficient to obtain an approximate solution that is a feasible solution of the original chance-constrained problem at a required level of confidence. Relevant theoretical results on the needed scenario sample size

are available also for non-convex problems in [23], including mixed-integer problems. In [23], an algorithm to determine a minimal number of scenarios to consider is provided, which can be computationally intensive. However, often a computationally feasible support sample can be found a posteriori, by adjusting the allowed violation levels considering a reasonable trade-off between computational and performance requirements. Furthermore, the uncertain constraints in the formulated MPC problem would be linear or affine, hence it would suffice replacing each chance constraint with one single deterministic approximate constraint. This will lead to a tractable SBMPC problem. This is currently being explored, as part of future works.

IV. Case Studies

A. System Configuration

The effectiveness of the proposed optimization framework is verified on a MES with 33-bus DN and 12-node 5G-DHC network. The configuration of the studied system is shown in Fig. 4. The DN parameters are taken from IEEE-33 bus system [24] and the 5G-DHC network parameters are obtained from [4] [19]. The allowed upper/lower bounds on voltage magnitudes in DN is set as 0.95 pu and 1.05 pu, respectively. The normalized renewable generation and load as well heating load in the 5G-DHC network are obtained from the National Renewable Energy Laboratory (NREL) Renewable Resource Data Center and Pecan Street dataset [25] [26]. These profiles are provided in Appendix, Fig. 7. The parameters for simulation setup are given in the Appendix, Table I. Case studies are performed in MATLAB with YALMIP toolbox [24] and the optimization problem is solved by Gurobi [27]. The prediction horizon for the case studies is 24 with a sampling period of 1 h. The average computational time for each MPC iteration is 4.45 s, on an Intel i5-12500H CPU (2.5 GHz clock frequency and 16GB RAM).

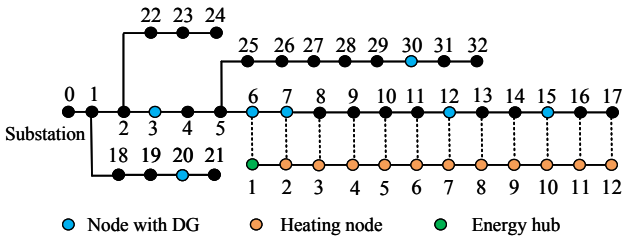

Fig. 4. Configuration of the studied system

B. Performance of Voltage Control

The voltage regulation capabilities of the proposed control framework with and without PTES are compared and the corresponding results are shown in Fig. 5a and Fig. 5b. Over-voltage issues occur in Fig. 5a, and highest voltage magnitude reaches 1.063 pu at 13:00 when there is high renewable generation. By contrast, the bus voltages are always regulated within the allowed range in Fig. 5b when the PTES is utilized.

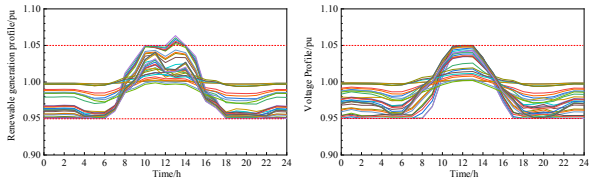

(a) without PTES. (b) with PTES.

Fig. 5. Performance of voltage control

C. Performance of Peak Shaving

The network peak load is also analyzed with and without PTES. The results are shown in Fig. 6a, where negative load denotes power flow from the DN to the substation. The peak load occurs at 20:00, and it is equal to 5.57 MW when the PTES is not used. The peak is 5.37 MW with PTES, hence it is reduced by 3.59%. The SOC of the mTIPTES is shown in Fig. 6b. The initial SOC level is set as 0.5. As it can been seen in Fig. 6b, when there is high load demand but low generation, the mTIPTES discharges to support the network load. The mTIPTES is charged to absorb excess electricity when there is high generation but low demand, as shown between 9:00 and 14:00 in Fig. 6b.

Over the 24-hour period, the total operational cost for the case without PTES amounts to $2092.39. With PTES integration, the operational cost decreases to $1911.50, yielding an improvement of approximately 8.65%. It is important to note the significance of this improvement. When contextualized in realistic scenarios with higher number of nodes and larger PTES capacity, it can lead to more impactful outcomes and significant peak and cost savingss.

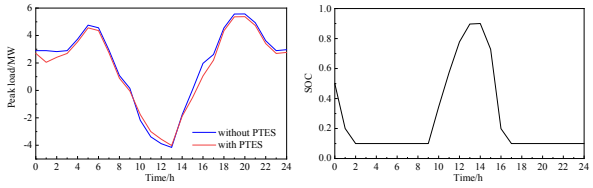

(a) Peak load in DN. (b) SOC of mTIPTES.

Fig. 6. Performance of peak shaving.

V. Conclusions

This paper proposed an optimization framework to use a PTES to provide simultaneous peak shaving and voltage control in MES. In the proposed framework, the operating characteristics of the PTES are linearized, and the dynamics of the PTES are handled by an MPC scheme. The overall optimization problem is formulated as a mixed-integer non-linear problem, which can be solved by off-the-shelf solvers. The results in the case studies show that an optimal use of a PTES integrated into a MES can lead to a reduced peak load as well as a reduction of the total operation cost, while the voltage is kept within the allowed limits. This demonstrates the promising potential of the PTES technology to support power networks with high penetration of renewable sources.

VI. Appendix

TABLE I
KEY PARAMETERS FOR SIMULATION SETUP

Parameter	Value
DN	
DG Capacity	1.2 MW
Electric Boiler	
Capacity	1500 kW
Efficiency	0.92
Electric Chiller	
Capacity	1000 kW
COP	5
5G-DHC Network	
WSHP COP	3.5
WSHP EER	4.0
WSHP Nominal Capacity	1300 kW
Warm Temperature	18 °C
Cold Temperature	12 °C
kA Value	2.5 W/mK
mTIPTES	
HTES Capacity	1600 kWh
Charging Time	4 h
Discharging Time	4 h
HTHP COP	5.9
ORC Efficiency	0.14
Minimum Load Level	0.4
Minimum/Maximum SOC Level	0.1/0.9

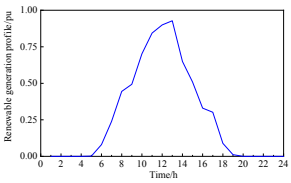

(a) Renewable generation profile.

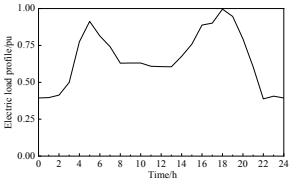

(b) Electric load profile.

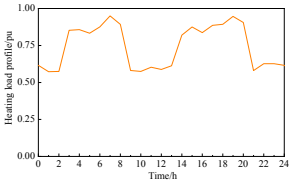

(c) Heating load profile.

Fig. 7. Generation/load Profiles.

References

[1] S. Bouckaert, A. F. Pales, C. McGlade, U. Remme, B. Wanner, L. Varro, D. D'Ambrosio, and T. Spencer, "Net zero by 2050: A roadmap for the global energy sector," 2021.

[2] H. B. Eluri and M. G. Naik, "Challenges of res with integration of power grids, control strategies, optimization techniques of microgrids: A review," *International Journal of Renewable Energy Research (IJRER)*, vol. 11, no. 1, pp. 1–19, 2021.

[3] E. Guelpa, A. Bischi, V. Verda, M. Chertkov, and H. Lund, "Towards future infrastructures for sustainable multi-energy systems: A review," *Energy*, vol. 184, pp. 2–21, 2019.

[4] M. Bilardo, F. Sandrone, G. Zanzottera, and E. Fabrizio, "Modelling a fifth-generation bidirectional low temperature district heating and cooling (5GDHC) network for nearly zero energy district (nZED)," *Energy Reports*, vol. 7, pp. 8390–8405, 2021.

[5] A. Castillo and D. F. Gayme, "Grid-scale energy storage applications in renewable energy integration: A survey," *Energy Conversion and Management*, vol. 87, pp. 885–894, 2014.

[6] W.-D. Steinmann, D. Bauer, H. Jockenhöfer, and M. Johnson, "Pumped thermal energy storage (PTES) as smart sector-coupling technology for heat and electricity," *Energy*, vol. 183, pp. 185–190, 2019.

[7] W. Tian and H. Xi, "Comparative analysis and optimization of pumped thermal energy storage systems based on different power cycles," *Energy Conversion and Management*, vol. 259, p. 115581, 2022.

[8] J. Martinek, J. Jorgenson, and J. D. McTigue, "On the operational characteristics and economic value of pumped thermal energy storage," *Journal of Energy Storage*, vol. 52, p. 105005, 2022.

[9] J. D. McTigue, P. Farres-Antunez, C. N. Markides, A. J. White, *et al.*, "Techno-economic analysis of recuperated joule-brayton pumped thermal energy storage," *Energy Conversion and Management*, vol. 252, p. 115016, 2022.

[10] H. Yang, J. Li, Z. Ge, L. Yang, and X. Du, "Dynamic performance for discharging process of pumped thermal electricity storage with reversible brayton cycle," *Energy*, vol. 263, p. 125930, 2023.

[11] H. Zhang, L. Wang, X. Lin, and H. Chen, "Combined cooling, heating, and power generation performance of pumped thermal electricity storage system based on brayton cycle," *Applied Energy*, vol. 278, p. 115607, 2020.

[12] G. F. Frate, L. Ferrari, P. Sdringola, U. Desideri, and A. Sciacovelli, "Thermally integrated pumped thermal energy storage for multi-energy districts: Integrated modelling, assessment and comparison with batteries," *Journal of Energy Storage*, vol. 61, p. 106734, 2023.

[13] M. Uddin, M. F. Romlie, M. F. Abdullah, S. Abd Halim, T. C. Kwang, *et al.*, "A review on peak load shaving strategies," *Renewable and Sustainable Energy Reviews*, vol. 82, pp. 3323–3332, 2018.

[14] H. Sun, Q. Guo, J. Qi, V. Ajjarapu, R. Bravo, J. Chow, Z. Li, R. Moghe, E. Nasr-Azadani, U. Tamrakar, *et al.*, "Review of challenges and research opportunities for voltage control in smart grids," *IEEE Transactions on Power Systems*, vol. 34, no. 4, pp. 2790–2801, 2019.

[15] J. Carden and D. Popovic, "Closed-loop volt\/var optimization: addressing peak load reduction," *IEEE Power and Energy Magazine*, vol. 16, no. 2, pp. 67–75, 2018.

[16] Y. Guo, Q. Zhang, and Z. Wang, "Cooperative peak shaving and voltage regulation in unbalanced distribution feeders," *IEEE Transactions on Power Systems*, vol. 36, no. 6, pp. 5235–5244, 2021.

[17] H. T. Nguyen and D.-H. Choi, "Three-stage inverter-based peak shaving and volt-var control in active distribution networks using online safe deep reinforcement learning," *IEEE Transactions on Smart Grid*, vol. 13, no. 4, pp. 3266–3277, 2022.

[18] M. E. Baran and F. F. Wu, "Optimal capacitor placement on radial distribution systems," *IEEE Transactions on Power Delivery*, vol. 4, no. 1, pp. 725–734, 1989.

[19] M. Wirtz, L. Kivilip, P. Remmen, and D. Müller, "5th generation district heating: A novel design approach based on mathematical optimization," *Applied Energy*, vol. 260, p. 114158, 2020.

[20] F. Bünning, M. Wetter, M. Fuchs, and D. Müller, "Bidirectional low temperature district energy systems with agent-based control: Performance comparison and operation optimization," *Applied Energy*, vol. 209, pp. 502–515, 2018.

[21] X. Xue, Y. Zhao, and C. Zhao, "Multi-criteria thermodynamic analysis of pumped-thermal electricity storage with thermal integration and application in electric peak shaving of coal-fired power plant," *Energy Conversion and Management*, vol. 258, p. 115502, 2022.

[22] T. Weller, H. Jockenhöfer, M. Fiss, and D. Bauer, "Detailed design of the high temperature tes laboratory prototype," *CHESTER H2020 project deliverable D*, vol. 3, p. 3, 2019.

[23] M. C. Campi, S. Garatti, and F. A. Ramponi, "A general scenario theory for nonconvex optimization and decision making," *IEEE Transactions on Automatic Control*, vol. 63, no. 12, pp. 4067–4078, 2018.

[24] J. Löfberg, "Yalmip : A toolbox for modeling and optimization in matlab," in *In Proceedings of the CACSD Conference*, (Taipei, Taiwan), 2004.

[25] "National renewable energy laboratory (NREL) https://www.nrel.gov/grid/solar-resource/renewable-resource-data.html."

[26] P. Street, "Pecan street dataport," *URL https://www. pecanstreet. org/dataport*, 2019.

[27] L. Gurobi Optimization, "Gurobi optimizer reference manual," 2020.